Research Article

Exosomes derived from human amniotic epithelial cells accelerate diabetic wound healing via PI3K-AKT-mTOR-mediated promotion in angiogenesis and fibroblast function

Pei Wei[1,2,3], **Chenjian Zhong**[1,2,3], **Xiaolan Yang**[1,2,3], **Futing Shu**[4,5], **Shichu Xiao**[4,5], **Teng Gong**[1,2,3], **Pengfei Luo**[4,5], **Li Li**[4,5], **Zhaohong Chen**[1,2,3,*], **Yongjun Zheng**[4,5,*], and **Zhaofan Xia**[1,2,3,4,5,*]

[1]Fujian Burn Institute, Fujian Medical University Union Hospital, Fuzhou 350001, Fujian, China, [2]Fujian Burn Medical Center, Fujian Medical University Union Hospital, Fuzhou 350001, Fujian, China, [3]Fujian Provincial Key Laboratory of Burn and Trauma, Fujian Medical University Union Hospital, Fuzhou 350001, Fujian, China, [4]Department of Burn Surgery, Changhai Hospital, Naval Medical University, Shanghai 200433, China and [5]Research Unit of key techniques for treatment of burns and combined burns and trauma injury, Chinese Academy of Medical Sciences, Changhai Hospital, Shanghai 200433, China

*Correspondence. Zhaofan Xia, Email: xiazhaofan_smmu@163.com; Yongjun Zheng, Email: smmuzhengyongjun@163.com; Zhaohong Chen, Email: doctorczh@163.com

Abstract

Background: Diabetic wounds are one of the most common and serious complications of diabetes mellitus, characterized by the dysfunction of wound-healing-related cells in quantity and quality. Our previous studies revealed that human amniotic epithelial cells (hAECs) could promote diabetic wound healing by paracrine action. Interestingly, numerous studies demonstrated that exosomes derived from stem cells are the critical paracrine vehicles for stem cell therapy. However, whether exosomes derived from hAECs (hAECs-Exos) mediate the effects of hAECs on diabetic wound healing remains unclear. This study aimed to investigate the biological effects of hAECs-Exos on diabetic wound healing and preliminarily elucidate the underlying mechanism.
Methods: hAECs-Exos were isolated by ultracentrifugation and identified by transmission electron microscopy, dynamic light scattering and flow cytometry. A series of *in vitro* functional analyses were performed to assess the regulatory effects of hAECs-Exos on human fibroblasts (HFBs) and human umbilical vein endothelial cells (HUVECs) in a high-glycemic microenvironment. High-throughput sequencing and bioinformatics analyses were conducted to speculate the related mechanisms of actions of hAECs-Exos on HFBs and HUVECs. Subsequently, the role of the candidate signaling pathway of hAECs-Exos in regulating the function of HUVECs and HFBs, as well as in diabetic wound healing, was assessed.
Results: hAECs-Exos presented a cup- or sphere-shaped morphology with a mean diameter of 105.89 ± 10.36 nm, were positive for CD63 and TSG101 and could be internalized by HFBs and HUVECs. After that, hAECs-Exos not only significantly promoted the proliferation and migration of

HFBs, but also facilitated the angiogenic activity of HUVECs *in vitro*. High-throughput sequencing revealed enriched miRNAs of hAECs-Exos involved in wound healing. Kyoto Encyclopedia of Genes and Genomes and Gene Ontology analyses have shown that the target genes of the top 15 miRNAs were highly enriched in the PI3K-AKT pathway. Further functional studies demonstrated that the PI3K-AKT-mTOR pathway was necessary for the induced biological effects of hAECs-Exos on HFBs and HUVECs, as well as on wound healing, in diabetic mice.

Conclusions: Our findings demonstrated that hAECs-Exos represent a promising, novel strategy for diabetic wound healing by promoting angiogenesis and fibroblast function via activation of the PI3K-AKT-mTOR pathway.

Background

Diabetic wounds are a common and serious complication of diabetes that not only increase the healthcare cost for our society but also cause physical dysfunction and psychological distress for patients [1].Conventional therapies, including blood glucose control, local blood circulation improvement, infection control and necrotic tissue removal, do not achieve satisfactory results [2]. Therefore, more effective therapeutic approaches are urgently needed.

Currently, stem cell therapy, a novel and advanced treatment, possesses a broad application prospect in the rehabilitation and regeneration of tissues and organs [3]. Human amniotic epithelial cells (hAECs) are derived from the placental amniotic membrane and characterized by non-tumorigenicity, low immunogenicity and are easy to isolate in large quantities [4]. Our previous study demonstrated that hAECs possessed powerful stem cell properties and could significantly accelerate diabetic wound healing [5]. However, the difficulty in preservation and limited transplantation activity make the practical application of hAECs problematic [6]. Interestingly, an increasing number of studies have shown that it is the paracrine mechanism of stem cells that mainly contributes to their therapeutic effects on tissue/organ regeneration, particularly extracellular vesicles [7]. Generally, extracellular vesicles can be divided into microvesicles, exosomes and apoptotic bodies, of which exosomes are secreted by nearly all cells and have been proved to play a central role in intercellular communication by delivering micro RNAs (miRNAs) and proteins from donor cells to recipient cells [8]. Moreover, owing to their great biocompatibility and low immunogenicity, exosomes are able to evade elimination by the reticuloendothelial and immune systems, thus maintaining the function of maternal cells for a long time [9]. Previous studies revealed that exosomes derived from human endothelial progenitor cells [10], human umbilical cord blood [11] and mesenchymal stem cells [12,13] could dramatically facilitate wound healing by modulating the function of human fibroblasts (HFBs) and human umbilical vein endothelial cells (HUVECs). However, whether exosomes derived from hAECs (hAECs-Exos) could serve as a novel alternative vehicle and fully exert the therapeutic effects of hAECs to promote diabetic wound healing has yet to be determined.

In this study, we detected the biological effects of hAECs-Exos on the activities of HFBs and HUVECs, profiled the expression of miRNAs in hAECs-Exos and speculated the candidate signaling pathway that mediate the function of hAECs-Exos. Meanwhile, the role of the candidate pathway in the induced effects of hAECs-Exos on the activities of HFBs and HUVECs, as well as on diabetic wound healing, was assessed. Our study aimed to explore the beneficial effects of hAECs-Exos on diabetic wound healing and to preliminarily elucidate the underlying mechanism.

Methods

Cell isolation and culture

All participants signed informed consent forms and all procedures were approved by the Ethics Committee of Changhai hospital, Shanghai, China. Human amniotic membranes were collected from healthy parturient women without genetic or infectious diseases. hAECs were isolated by Shanghai iCELL Biotechnology Co., Ltd (China) as previously reported [5] and cultured in Dulbecco's modified Eagle's medium (DMEM; Gibco, USA) with a glucose concentration of 5.5 mmol/L and supplemented with 10% fetal bovine serum (FBS; Gibco, USA) and 2% penicillin/streptomycin. HFBs were isolated from neonatal human foreskin according to generally accepted methods [14]. HUVECs were purchased from the China Center for Type Culture Collection (China). Both HFBs and HUVECs were cultured in high-glucose DMEM with a glucose concentration of 33 mmol/L to mimic a hyperglycemic environment, supplemented with 10% FBS and 2% penicillin/streptomycin. All of these cells were maintained at 37°C with 5% CO_2 in a humidified atmosphere, and cells at passages 2–6 were used for further experiments.

Isolation and identification of hAECs-Exos

When cell confluence reached 70–80%, hAECs were washed with phosphate-buffered saline (PBS) and incubated with DMEM containing 10% exosome-free FBS for 48 hours. The conditioned medium was collected, successively centrifuged at $300 \times g$ for 10 minutes, $2000 \times g$ for 10 minutes and $10,000 \times g$ for 30 minutes to remove dead cells and cell

fragments, and finally passed through a 0.22 um filter (Millipore, Billerica, USA). Next, the filtrate was centrifuged at $100,000 \times g$ for 2 hours, washed twice with 500 µL PBS and recentrifuged at $100,000 \times g$ for 2 hours to collect pure exosomes. All procedures were conducted at 4°C. Exosomes suspended in 100 µL PBS were stored at −80°C for further experiments. The size distribution of hAECs-Exos was analysed by dynamic light scattering (DLS) with a Malvern Nanosizer (Malvern Instruments, UK). The morphology of hAECs-Exos was observed by transmission electron microscope (TEM) (Hitachi H-7650; Hitachi, Japan) as described previously in detail [10]. The surface markers (CD63, TSG101) of hAECs-Exos were analysed by flow cytometry (FCM) with the primary antibodies mouse anti-human CD63 (Santa Cruz Biotechnology, USA) and rabbit anti-human TSG101 (ProteinTech, USA) as described previously [11]. Finally, the protein level of hAECs-Exos was quantified with a Pierce BCA Protein Assay Kit (Thermo Fisher Scientific, USA) for subsequent studies.

Labeling and internalization assay of hAECs-Exos
Exosomes were labeled with PKH26 (Sigma, USA) according to the manufacturer's instructions [15] and incubated with HFBs or HUVECs in the dark at 37°C for 3 hours. Subsequently, the cells were washed with PBS 3 times and fixed with 4% paraformaldehyde for 15 minutes. Finally, cell nuclei were stained with 0.5 µg/ml 4′,6-diamidino-2-phenylindole (Invitrogen, USA) and observed with an inverted fluorescence microscope (Leica, Germany).

In vitro effects of hAECs-Exos on HFBs and HUVECs
For examining the effects of hAECs-Exos on the actions of HFBs and HUVECs, the cells were cultured and received different treatments: (1) Control group (treated with an equal volume of hAECs-Exos diluent (PBS)); and (2) hAECs-Exos group (treated with 100 µg/ml hAECs-Exos). For determining the role of phosphatidylinositol 3-kinase (PI3K)- protein kinase B (AKT) in the effects of hAECs-Exos on the activities of HFBs and HUVECs, they were treated with different methods: (1) DMSO + PBS group (treated with an equal volume of LY294002 diluent dimethyl sulfoxide (DMSO) + PBS); (2) DMSO + hAECs-Exos group (treated with DMSO + hAECs-Exos (100 µg/ml)); and (3) LY294002 + hAECs-Eos group (treated with LY294002 (2.5 µmol/l) + hAECs-Exos (100 µg/ml)).

Cell proliferation assay
Briefly, 5×10^3 cells were seeded into 96-well plates, cultured in exosome-free low-serum (2.5% FBS) medium and treated with different methods according to the experimental purpose. Culture medium without cells acted as the blank group. On hours 0, 12, 24, 36, 48 and 60, cell counting kit-8 reagent (CCK-8; 10 µL per well; Dojindo, Japan) was added to each culture medium (100 µL per well). Three repeated measurement wells were set for each point. After incubation

at 37°C for 2.5 hours, the absorbance was evaluated at 450 nm by a microplate reader (ELx800, BioTek, USA). The cell proliferation was evaluated as the mean absorbance of repeated wells minus the blank value.

Scratch assay
Cells (5×10^5 cells/well) were seeded into 6-well plates, incubated to reach 100% confluence and starved overnight. Then, the monolayer was scratched with a p200 pipette tip and washed with PBS to remove floating cells. Subsequently, the cells were cultured in exosome-free low-serum (2.5% FBS) medium, treated with different medium according to the experimental purpose and photographed at indicated time points. Image-Pro Plus (Media Cybernetics, Rockville, MD, USA) was used to measure the wound area. The rate of migration was analysed according to the following formula: migration area (%) = (A0−At)/A0 × 100, where A0 indicates the area of the initial wound scratch and At indicates the remaining wound area at the measurement point.

Transwell assay
Cells (1×10^5) were suspended in exosome-free low-serum (2.5% FBS) medium and seeded into the upper compartment of a 24-well transwell chamber (Corning, USA) with 8 µm pore filters. The lower compartment was filled with exosome-free higher-serum (5% FBS) medium supplemented with different treatment according to the experimental purpose. After incubation for 24 hours, the cells attached to the upper surface were removed and the migrated cells attached to the lower surface were fixed with 4% formaldehyde and stained with 0.1% crystal violet (Solarbio, China) for 30 minutes. The images of migrated cells were gathered with an inverted microscope (Leica) and the number of migrated cells was counted by Image-Pro Plus.

Tube-formation assay
Each well of 96-well plates was covered with 60 µL Matrigel (BD Biosciences, USA) and incubated at 37°C for 30 minutes. Then, HUVECs (2×10^4 cells/well) were cultured with exosome-free complete medium and treated with different methods according to the experimental purpose. After incubating at 37°C for 6 hours, capillary-like structures were observed with an inverted microscope (Leica) and the total loop number was counted by Image-Pro Plus.

Western blotting analysis
Cells (5×10^5 cells/well) were seeded into 6-well culture plates overnight and then received different treatments according to the experimental purpose. After incubation for 24 hours, cells were lysed and proteins were collected by NCM RIPA buffer (New Cell & Molecular Biotech, China). The protein concentration was quantified by a Pierce BCA Protein Assay Kit (Thermo Fisher Scientific, USA). Western blot analysis was performed with primary antibodies against p-AKT (Cell Signaling Technology, USA), AKT (Cell Signaling Technology),

Table 1. The primer sequences for the top 15 miRNAs of hAECs-Exos-miRNAs

miRNAs	Primer sequences
hsa-miRNA-21-5p	CGCGTAGCTTATCAGACTGATGTTGA
hsa-miRNA-24-3p	TGGCTCAGTTCAGCAGGAAC
hsa-miRNA-423-5p	TGAGGGGCAGAGAGCGA
hsa-miRNA-320a-3p	AAAAGCTGGGTTGAGAGGGC
hsa-miRNA-26a-5p	CCGTTCAAGTAATCCAGGATAGGCT
hsa-miRNA-151a-3p	GCTAGACTGAAGCTCCTTGAGG
hsa-miRNA-122-5p	AGTGGAGTGTGACAATGGTGTTTG
hsa-miRNA-1246	GCGAATGGATTTTTGGAGCAGG
hsa-miRNA-181a-5p	AACATTCAACGCTGTCGGTGAG
hsa-miRNA-25-3p	CATTGCACTTGTCTCGGTCTGA
hsa-miRNA-99a-5p	CAACCCGTAGATCCGATCTTGTG
U6	F: CTCGCTTCGGCAGCACA
	R: AACGCTTCACGAATTTGCGT
Universal primer	TG CTGTCAACGATACGCTACG

F forward, *R* reverse, *hAECs* human amniotic epithelial cells

p-mammalian target of rapamycin (mTOR) (Cell Signaling Technology) and mTOR (Cell Signaling Technology) as previously described [16].

Microarray analysis
The miRNAs in hAECs-Exos were analysed using an Agilent miRNAs microarray by RiboBio Co., Ltd (China). The Kyoto Encyclopedia of Genes and Genomes (KEGG) and Gene Ontology (GO) analyses were performed by RiboBio Co., Ltd as well.

RT-qPCR analysis
Cells (5×10^5 cells/well) were seeded in 6-well culture plates overnight and incubated with hAECs-Exos (100 μg/ml) or PBS for 4 hours. Total miRNAs were extracted with the miRNeasy® mini Kit (QIAGEN, Germany) and reverse transcribed using the miRcute Plus miRNAs First-Strand cDNA Kit (TIANGEN, China). The RT-qPCR analysis was performed with SYBR® Premix Ex Taq II (TaKaRa, Japan) and the StepOne Plus Real-Time PCR System. The primer sequences are detailed in Table 1.

The expression of each miRNA was quantified through normalization to the internal reference U6, and the $2^{-\Delta\Delta CT}$ method was applied to determine the relative quantity.

In vivo effects of hAECs-Exos on diabetic wounds
All procedures were approved by the Animal Research Committee of Naval Medical University, Shanghai, China. Forty male db/db mice (C57BL/KsJ, leptin receptor-deficient diabetes, 8–12 weeks) were purchased from Slac Laboratory Animal Co. Ltd (China). The criterion for inclusion was a blood glucose level of >300 mg/dl. The mice were intraperitoneally anesthetized with 1% sodium pentobarbital and two full-thickness cutaneous wounds (8 mm in diameter) were created on the dorsum of each mouse. They were randomly divided into three treatment groups: (1) DMSO + PBS group (treated with an equal volume of LY294002 diluent (10% DMSO)

+ 200 μL PBS); (2) DMSO + hAECs-Exos group (treated with 10% DMSO + 200 μL hAECs-Exos (1000 μg/ml)); and (3) LY294002 + hAECs-Exos group (treated with LY294002 (2.5 mg/kg) + 200 μL hAECs-Exos (1000 μg/ml)). On day 18 post-operation, the mice were sacrificed and skin samples containing the wound beds and healthy tissues were harvested and divided into two sections along the diameter.

Evaluation of the wound-healing process
The wounds were photographed at days 0, 4, 8, 12 and 14 after wounding, and the wound area was evaluated by Image-Pro Plus software. The wound-closure rate was calculated as follows: wound-closure rate (%) = (A0−At)/A0 × 100 (A0, the original wound area; At, the wound area at the indicated time).

Hematoxylin-eosin and Masson's trichrome staining
Skin specimens were fixed overnight in 4% paraformaldehyde, dehydrated with a series of graded ethanol, embedded in paraffin and then cut into 5-mm sections. For histological analysis, wound sections were stained with hematoxylin-eosin (H&E) and Masson's trichrome staining. Full thickness of healing skin was evaluated by Image-Pro Plus.

Immunohistochemistry and picrosirius red staining
Slides were prepared as previously involved in H&E and Masson's trichrome staining. Three sections from each group were performed for immunohistochemistry as described previously [17]. The primary antibodies, including antibodies against collagen 1A1 (Abcam, USA), collagen 3A1 (Abcam) and CD31 (Abcam) were used in immunohistochemistry. Digital images were obtained by microscope (Leica) and the intensity of each item was evaluated by Image-Pro Plus. Meanwhile, three slices of each group were stained with picrosirius red to assess the collagen volume fraction. Digital images were acquired with a polarized microscope. Collagen volume fraction for each group was evaluated by Image-Pro Plus software.
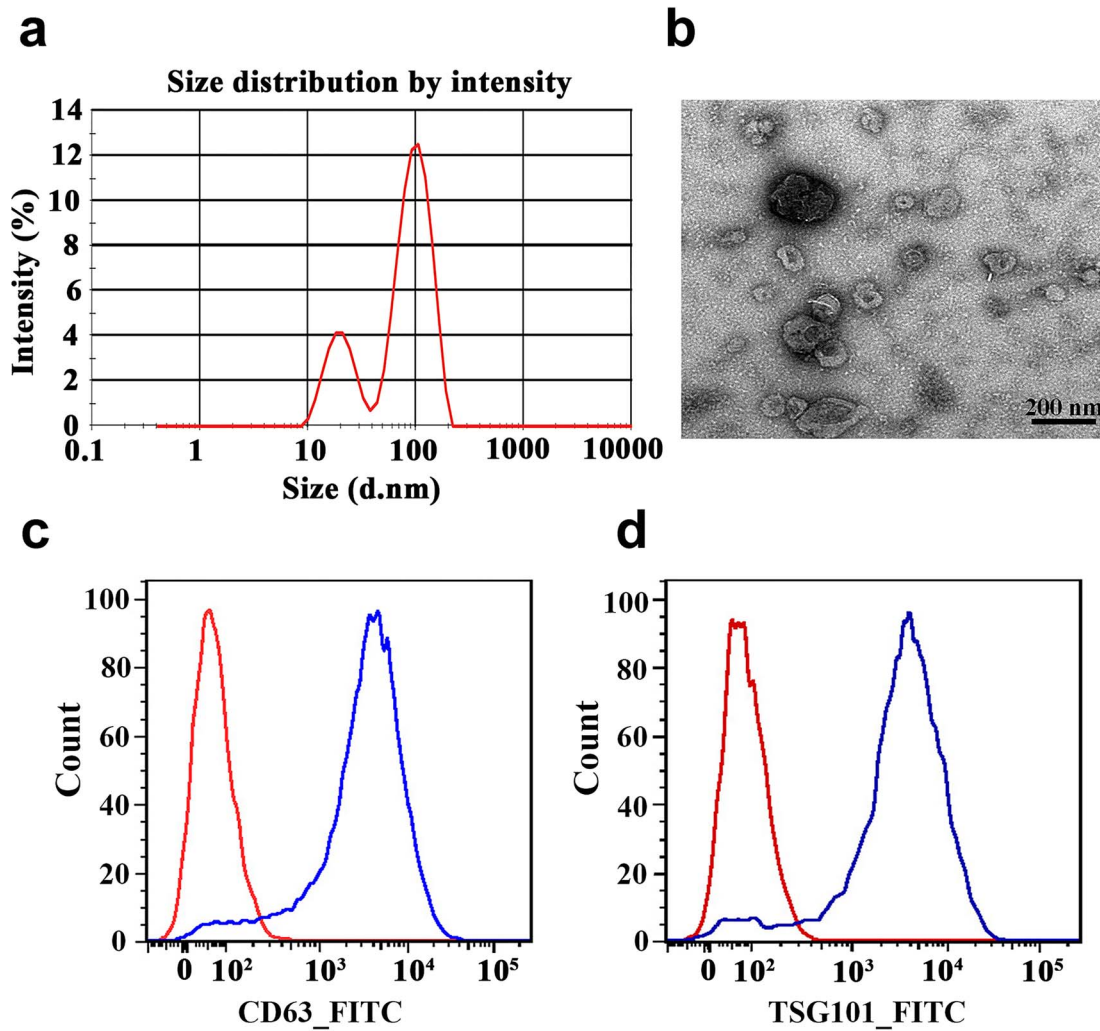
Figure 1. Characterization of hAECs-Exos. **(a)** The particle size distribution of hAECs-Exos was analyzed by dynamic light scattering. **(b)** The morphology of hAECs-Exos was viewed by transmission electron microscope. Scale bar: 200 nm. **(c)** Surface marker CD63 of hAECs-Exos was detected by flow cytometry. **(d)** Surface marker TSG101 of hAECs-Exos was detected by flow cytometry, as well. Red curves represent the isotype control and blue curves represent CD63 or TSG101. *hAECs-Exos* exosomes derived from human amniotic epithelial cells

Statistical analysis

SPSS 16.0 software was used for statistical analysis and the results were expressed as the mean $\pm$ SD. Differences between two groups were analysed with Student's t test, differences between three groups were analysed with one-way analysis of variance (ANOVA) and differences between two or three groups at different time points were evaluated with two-way ANOVA. A p value of <0.05 was statistically significant.

Results

Isolation and identification of hAECs-Exos

hAECs-Exos were isolated by ultracentrifugation and identified by DLS, TEM and FCM. DLS measurement revealed that the mean diameter of hAECs-Exos was 105.89 ± 10.36 nm (Figure 1a), which was located in the previously reported exosome diameter range of 50–150 nm.

TEM demonstrated that hAECs-Exos exhibited cup- and sphere-shaped morphologies (Figure 1b). Furthermore, FCM showed the presence of the exosomal markers CD63 and TSG101 (Figure 1c, d). All these results indicated that hAECs-Exos were successfully isolated from hAECs-conditioned medium.

hAECs-Exos facilitated the proliferation of HFBs and HUVECs

As shown in Figure 2a, b, PKH26-labeled hAECs-Exos were transferred to the perinuclear region of HFBs and HUVECs after co-incubation for 3 hours. The CCK-8 assay revealed that the proliferation of HFBs and HUVECs was significantly accelerated by hAECs-Exos from 12 hours (Figure 2c, d). These data specifically confirmed that hAECs-Exos were successfully absorbed by HFBs and HUVECs and significantly accelerated cell proliferation.
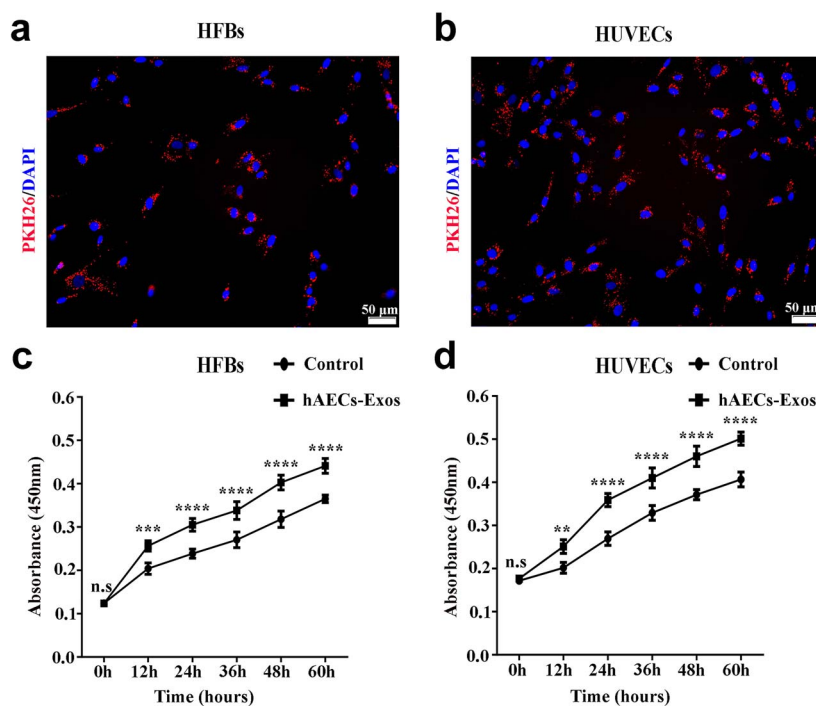
Figure 2. hAECs-Exos promoted the proliferation of HFBs and HUVECs. **(a–b)** PKH26-labeled hAECs-Exos were absorbed and concentrated in the perinuclear region of HFBs **(a)** and HUVECs **(b)**, respectively. Scale bars: 50 μm. **(c)** The proliferative effect of hAECs-Exos on HFBs was evaluated by the cell counting kit-8 assay. **(d)** Counting kit-8 assay was applied to detect the proliferation of HUVECs treated with hAECs-Exos. $**p < 0.01$, $***p < 0.001$, $****p < 0.0001$. *n.s* no significance, *hAECs-Exos* exosomes derived from human amniotic epithelial cells, *HFBs* human fibroblasts, *HUVECs* human umbilical vein endothelial cells
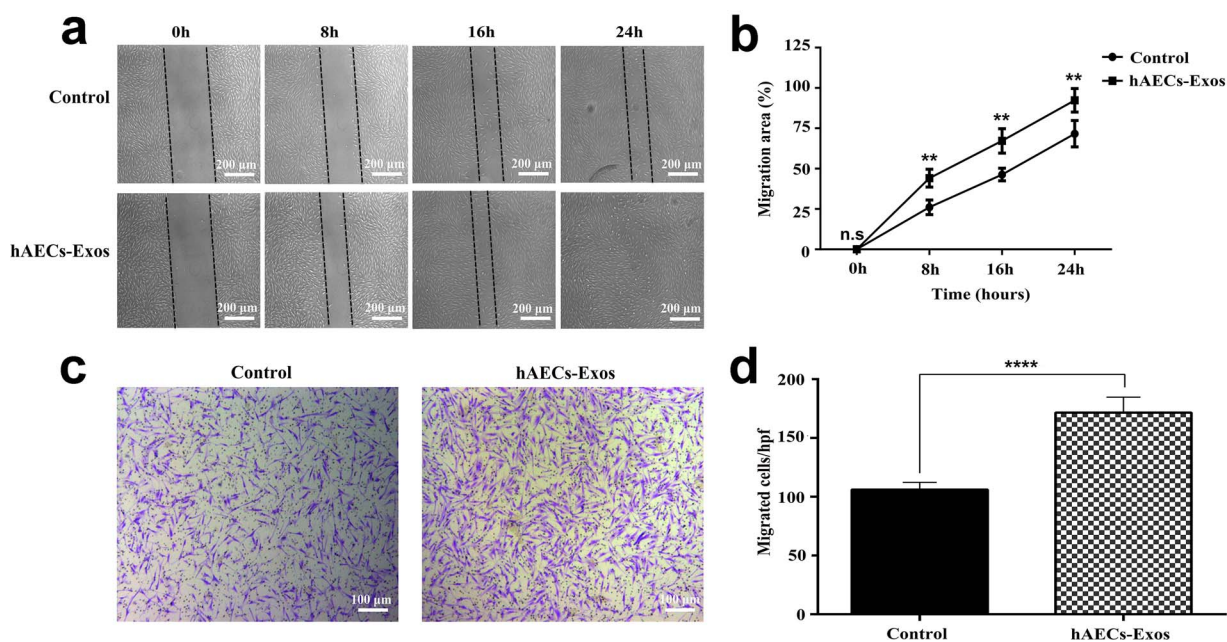
Figure 3. hAECs-Exos facilitated the migration of HFBs. **(a)** Representative images of the scratch assay in HFBs treated with hAECs-Exos or an equal volume of PBS. Scale bars: 200 μm. **(b)** Quantitative analysis of the migration rate in **(a)**. **(c)** The migration effect of hAECs-Exos on HFBs was detected by the transwell assay. **(d)** Quantitative analysis of the migrated cells in **(c)**. Scale bars: 100 μm. $**p < 0.01$, $****p < 0.0001$. *n.s* no significance, *hAECs-Exos* exosomes derived from human amniotic epithelial cells, *HFBs* human fibroblasts
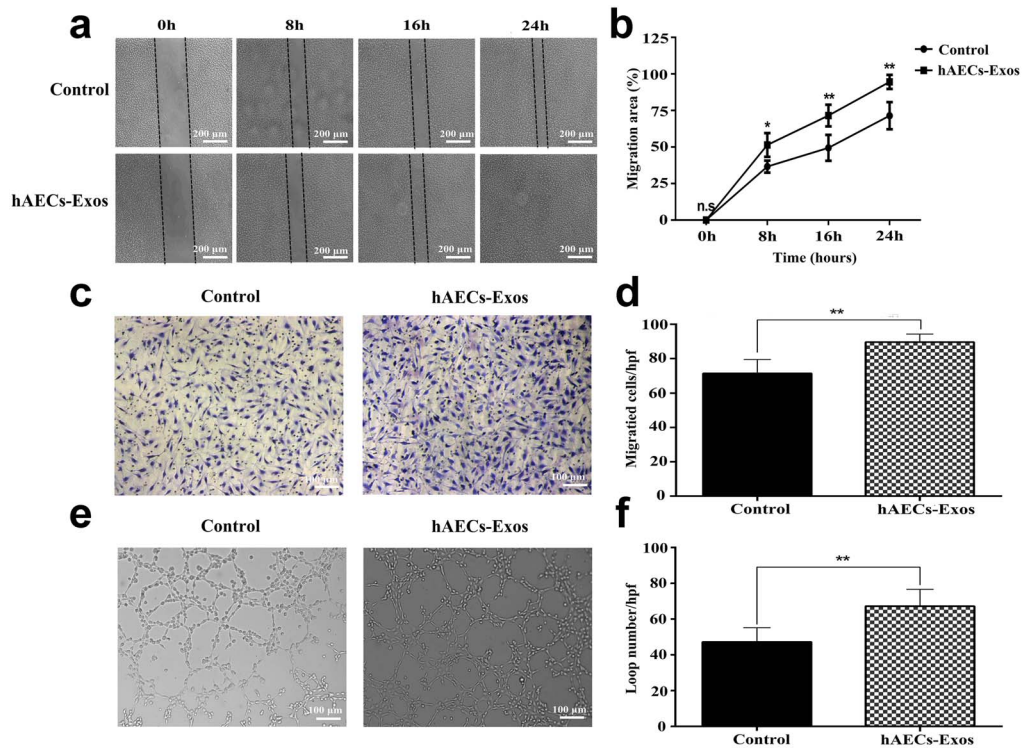
Figure 4. hAECs-Exos facilitated the angiogenic activities of HUVECs. **(a)** HUVECs exhibited enhanced migration ability when exposed to hAECs-Exos, as demonstrated by scratch analysis. Scale bars: 200 μm **(b)** Quantitative analysis of the migration rate in **(a)**. **(c)** Transwell assay revealed that hAECs-Exos up-regulated the motility of HUVECs as well. Scale bars: 100 μm. **(d)** Quantitative analysis of the migrated cells in **(c)**. **(e)** Representative images of the tube-formation assay on Matrigel in HUVECs treated with hAECs-Exos or PBS. Scale bars: 100 μm. **(f)** Quantitative analysis of total loops in **(e)**. $*p < 0.05$, $**p < 0.01$. *n.s* no significance, *hAECs-Exos* exosomes derived from human amniotic epithelial cells, *HUVECs* human umbilical vein endothelial cells, *PBS* phosphate buffer saline
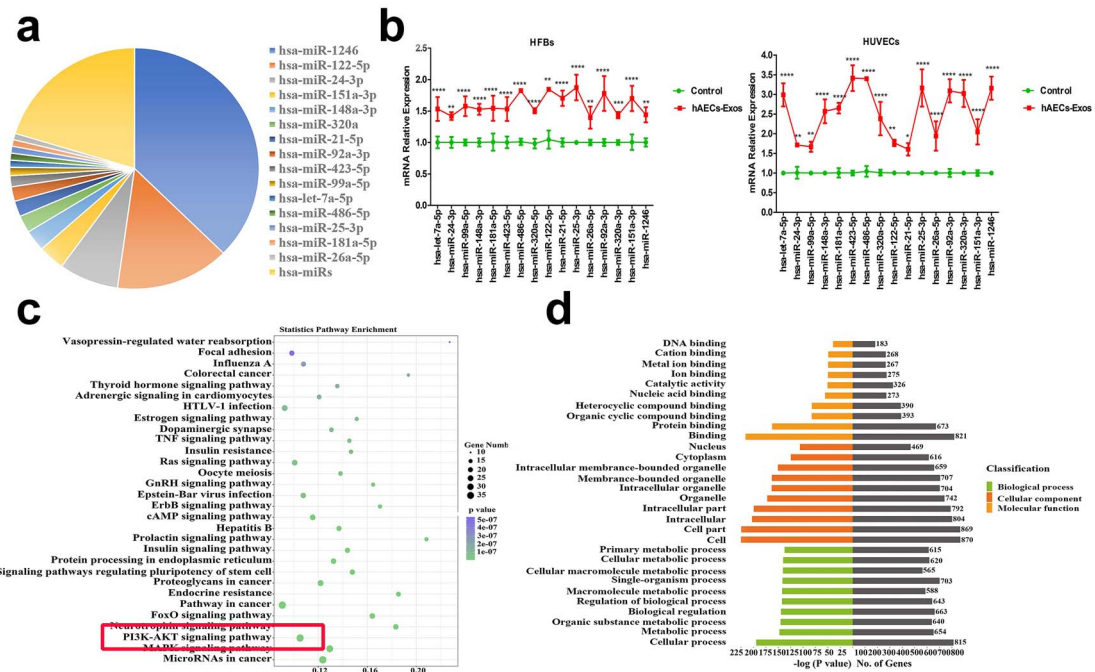

Figure 5. miRNAs profile of hAECs-Exos and enrichment pathway analysis. **(a)** The top 15 miRNAs in hAECs-Exos were color labeled. **(b)** The expression levels of the top 15 hAECs-Exos-miRNAs in HUVECs and HFBs treated with hAECs-Exos were quantified by RT-qPCR. **(c)** Enriched signaling pathways of the target genes for the top 15 miRNAs were analyzed by Kyoto Encyclopedia of Genes and Genomes. **(d)** The biological processes of the target genes for the top 15 miRNAs were analyzed by Gene Ontology. *hAECs-Exos* exosomes derived from human amniotic epithelial cells, *miRNAs* micro RNAs, *HFBs* human fibroblasts, *HUVECs* human umbilical vein endothelial cells, *RT-qPCR* real time quantitative polymerase chain reaction
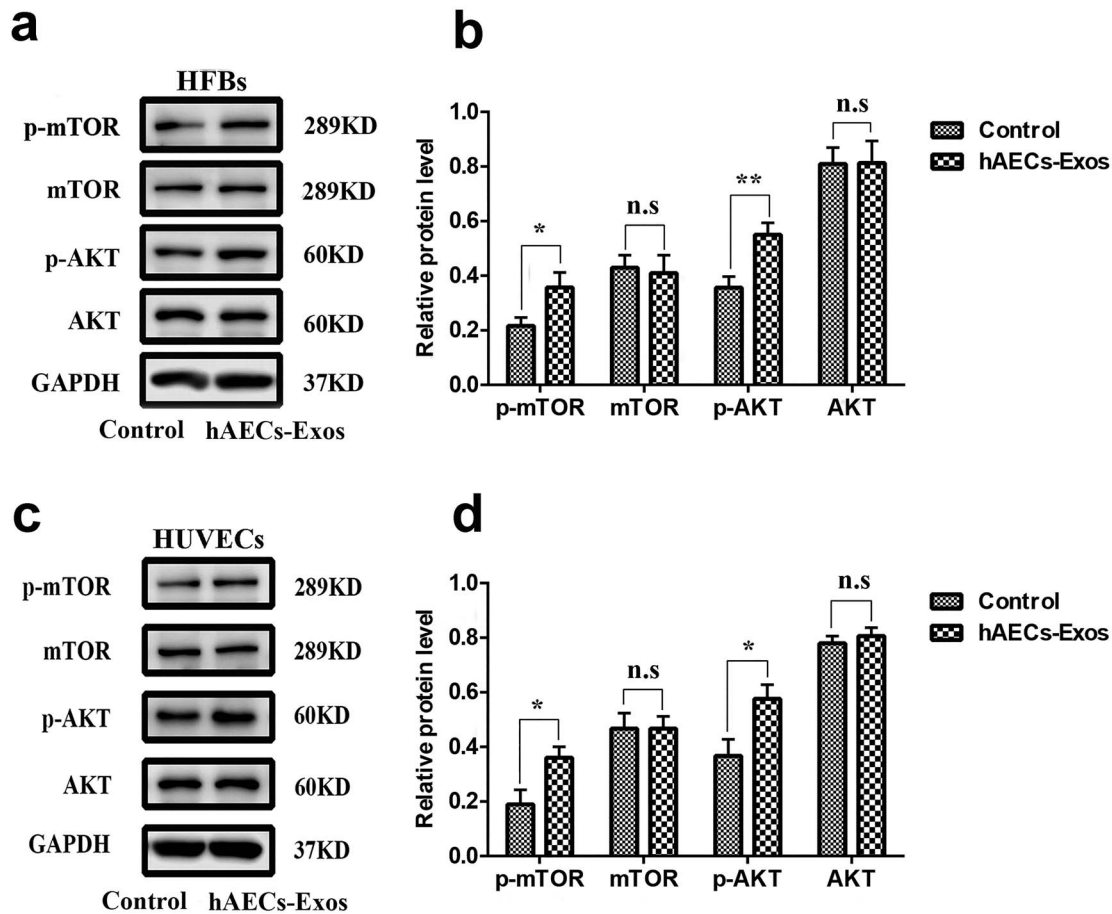
Figure 6. PI3K-AKT-mTOR was activated in HFBs and HUVECs treated with hAECs-Exos. **(a)** The protein levels of AKT, p-AKT, mTOR and p-mTOR in HFBs treated with hAECs-Exos or PBS, as tested by western blotting. **(b)** Quantitative analysis of the relative protein level in **(a)**. **(c)** The protein levels of p-AKT and p-mTOR were enhanced in HUVECs when exposed to hAECs-Exos. **(d)** Quantitative analysis of the relative protein level in **(c)**. *$p < 0.05$, **$p < 0.01$. *n.s* no significance, *hAECs-Exos* exosomes derived from human amniotic epithelial cells, *PBS* phosphate buffer saline, *PI3K-AKT-mTOR* phosphatidylinositol 3 kinase-protein kinase B-mammalian target of rapamycin, *p-mTOR* phosphorylated mammalian target of rapamycin, *p-AKT* phosphorylated protein kinase B

hAECs-Exos facilitated the migration of HFBs

The migration of HFBs is as important as their proliferation for wound healing. Both scratch assays and transwell assays were conducted to evaluate the promoting effect of hAECs-Exos on HFB migration (Figure 3a–d). Scratch analysis demonstrated that hAECs-Exos remarkably upregulated the migration of HFBs ($p < 0.01$), which was consistent with the result of the transwell assays ($p < 0.0001$).

hAECs-Exos enhanced the angiogenic activities of HUVECs

Angiogenesis is another important factor in wound healing, as it provides nutritional support to the wound sites. In addition to the obvious proliferation effect, both scratch assay (Figure 4a, b) and transwell assay (Figure 4c, d) revealed that hAECs-Exos strongly stimulated the migration ability of HUVECs. The tube-formation assay on Matrigel is a universally recognized model of angiogenesis *in vitro*. As shown in Figure 4e, f, HUVECs treated with hAECs-Exos showed a greater number of capillary-like structures

compared with the control group ($p < 0.01$). These results illustrated that hAECs-Exos could remarkably promote the angiogenic activities of HUVECs

miRNA profile of hAECs-Exos and enrichment analysis of pathway

An increasing number of studies have reported that the primary functional cargo of exosomes is the group of miRNAs which can be efficiently internalized by recipient cells and modulate their biological behaviors [18]. We analysed the miRNA profile in hAECs-Exos (shown in supplementary data) and the top 15 miRNAs are indicated in Figure 5a. When HFBs and HUVECs were co-incubated with hAECs-Exos for 4 hours,the expression of the top 15 miRNAs were significantly upregulated (Figure 5b). These data indicated that hAECs-Exos-miRNAs could be successfully transferred into HFBs and HUVECs. Then, KEGG (Figure 5c) and GO (Figure 5d) analyses were carried out to predict the enrichment pathways and biological processes of their target genes. KEGG assay demonstrated that the PI3K-AKT
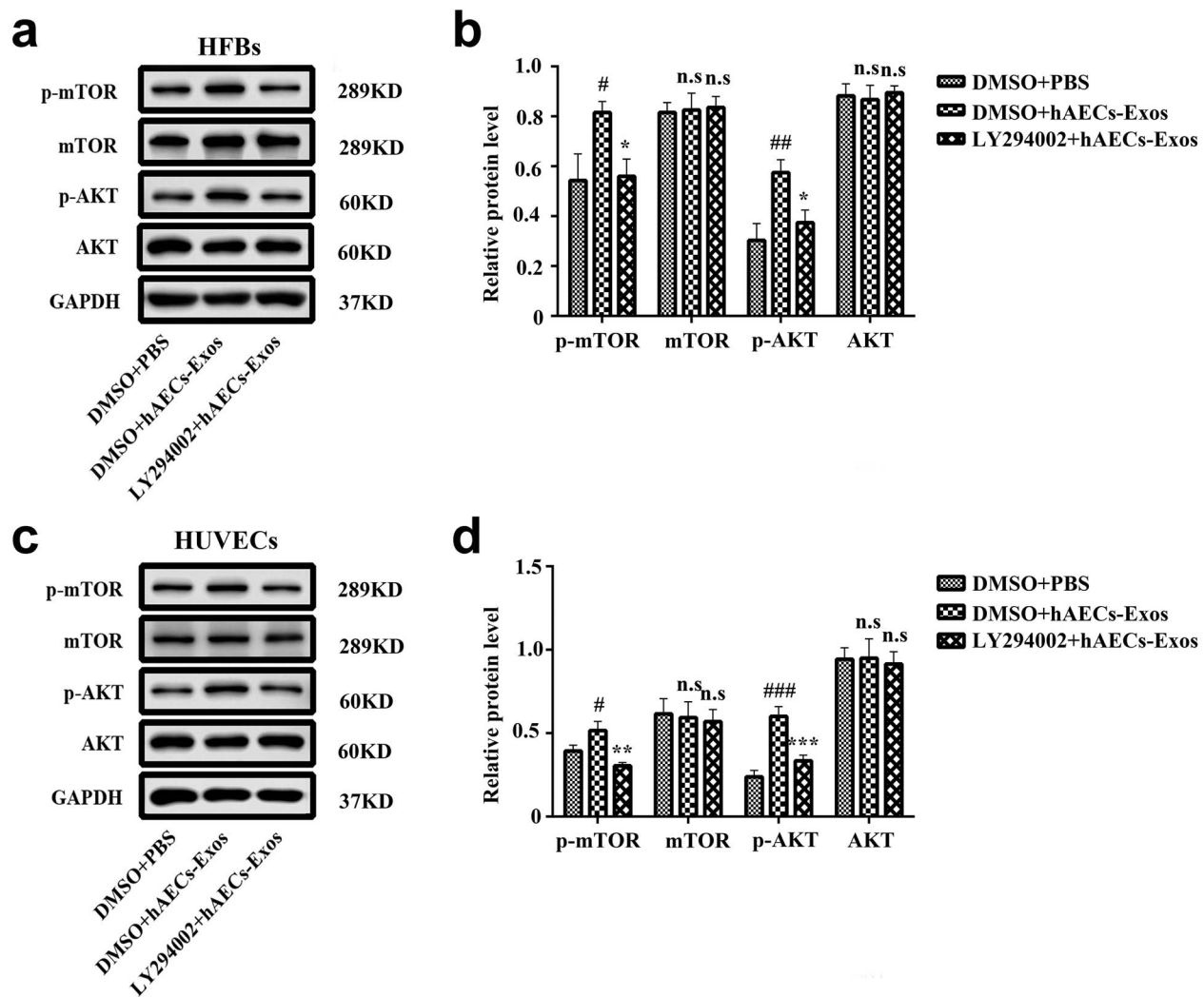
Figure 7. PI3K-AKT-mTOR activated in HFBs and HUVECs was inhibited by LY294002. **(a)** Western blotting was applied to detect the protein expressions of AKT, p-AKT, mTOR and p-mTOR in HFBs treated with DMSO + hAECs-Exos, DMSO + PBS and LY294002 + hAECs-Exos. **(b)** Quantitative analysis of the relative protein level in **(a)**. **(c)** LY294002 decreased the expression level of p-AKT and p-mTOR in HUVECs upregulated by hAECs-Exos. **(d)** Quantitative analysis of the relative protein level in **(c)**. $*p < 0.05$, $**p < 0.01$, $***p < 0.001$ compared with DMSO + hAECs-Exos group, $^\#p < 0.05$, $^{\#\#}p < 0.01$, $^{\#\#\#}p < 0.001$ compared with the DMSO + PBS group. *n.s* no significance, *hAECs-Exos* exosomes derived from human amniotic epithelial cells, *DMSO* Dimethyl Sulfoxide, *PBS* phosphate buffer saline, *PI3K-AKT-mTOR* phosphatidylinositol 3 kinase-protein kinase B-mammalian target of rapamycin, *p-mTOR* phosphorylated mammalian target of rapamycin, *p-AKT* phosphorylated protein kinase B

signaling pathways were highly enriched. Moreover, western blotting analysis verified that the expression levels of p-AKT and p-mTOR were indeed significantly increased in HFBs and HUVECs after treatment with hAECs-Exos (Figure 6).

PI3K-AKT-mTOR mediated the biological effects of hAECs-Exos on HFBs and HUVECs

To investigate the role of PI3K-AKT-mTOR in the effects of hAECs-Exos on HFBs and HUVECs, LY294002 was used to selectively block PI3K-AKT-mTOR in hAECs-Exos-treated cells. Results of the western blotting assay revealed that the protein levels of p-AKT and p-mTOR were significantly increased in HFBs and HUVECs treated with hAECs-Exos. However, when LY294002 was added to the hAECs-Exos treatment system, the protein expressions of p-AKT and p-mTOR were obviously downregulated (Figure 7).

These data demonstrated that PI3K-AKT-mTOR is directly activated by hAECs-Exos in HFBs and HUVECs, and that this effect could be blocked by LY294002. CCK-8 assay showed a weakened power of hAECs-Exos to increase the proliferation of HFBs and HUVECs when the PI3K-AKT-mTOR pathway was blocked in them (Figure 8a, b). As evidenced by the transwell assay (Figure 8c–f), the pro-migratory effects of hAECs-Exos on HFBs and HUVECs were also suppressed once the PI3K-AKT-mTOR pathway was blocked in HFBs and HUVECs. Meanwhile, tube-formation assay showed fewer numbers of capillary-like structures on Matrigel with HUVECs treated with LY294002 + hAECs-Exos compared with the DMSO + hAECs-Exos group (Figure 9). These data revealed that PI3K-AKT-mTOR mediated the biological effects of hAECs-Exos on HFBs and HUVECs.
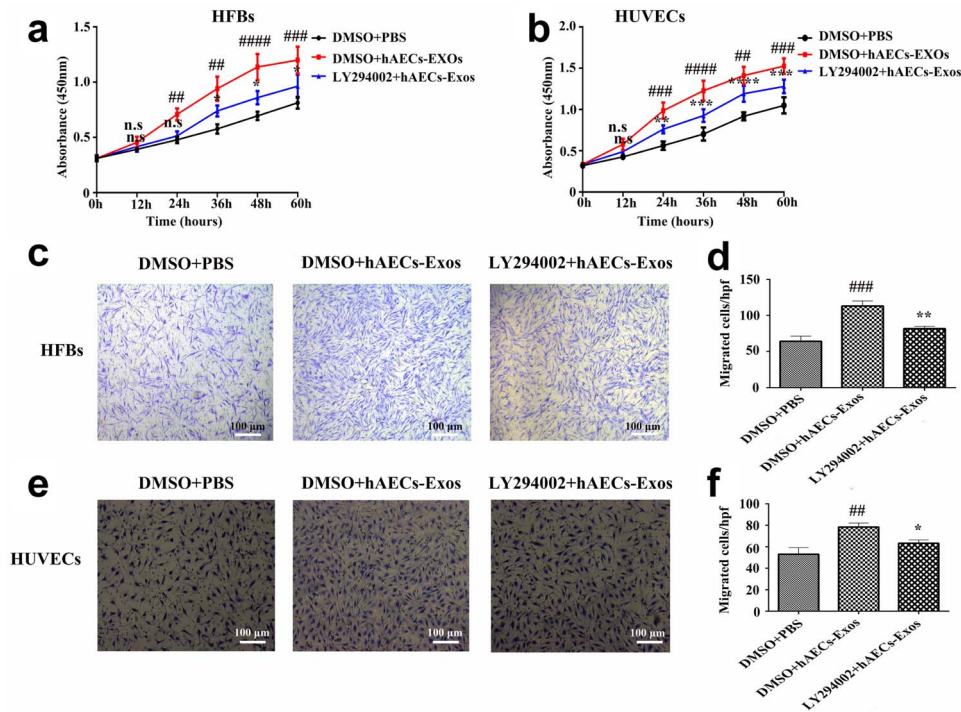
Figure 8. PI3K-AKT-mTOR mediated the proliferation and migration effects of hAECs-Exos on HFBs and HUVECs. **(a)** The proliferation of HFBs treated with DMSO + hAECs-Exos, DMSO + PBS and LY294002 + hAECs-Exos was demonstrated by cell counting kit-8 analysis. **(b)** Counting kit-8 assay was applied to detect the proliferation of HUVECs treated with DMSO + hAECs-Exos, DMSO + PBS and LY294002 + hAECs-Exos, as well. **(c)** The migration ability of HFBs stimulated by DMSO + hAECs-Exos, DMSO + PBS and LY294002 + hAECs-Exos was detected by transwell assay. **(d)** Quantitative analysis of the migrated cells in **(c)**. **(e)** The transwell assay was applied to detect the migration ability of HUVECs stimulated with DMSO + hAECs-Exos, DMSO + PBS and LY294002 + hAECs-Exos. **(f)** Quantitative analysis of the migrated cells in **(e)**. Scale bars: 100 μm. *p<0.05, **p<0.01, ***p<0.001, ****p<0.0001 compared with DMSO+hAECs-Exos group, ##p<0.01 ###p<0.001, ####p<0.0001 compared with the DMSO+PBS group. *n.s* no significance, *DMSO* Dimethyl Sulfoxide, *PBS* phosphate buffer saline, *PI3K-AKT-mTOR* phosphatidylinositol 3 kinase-protein kinase B-mammalian target of rapamycin, *hAECs-Exos* exosomes derived from human amniotic epithelial cells, *HFBs* human fibroblasts, *HUVECs* human umbilical vein endothelial cells
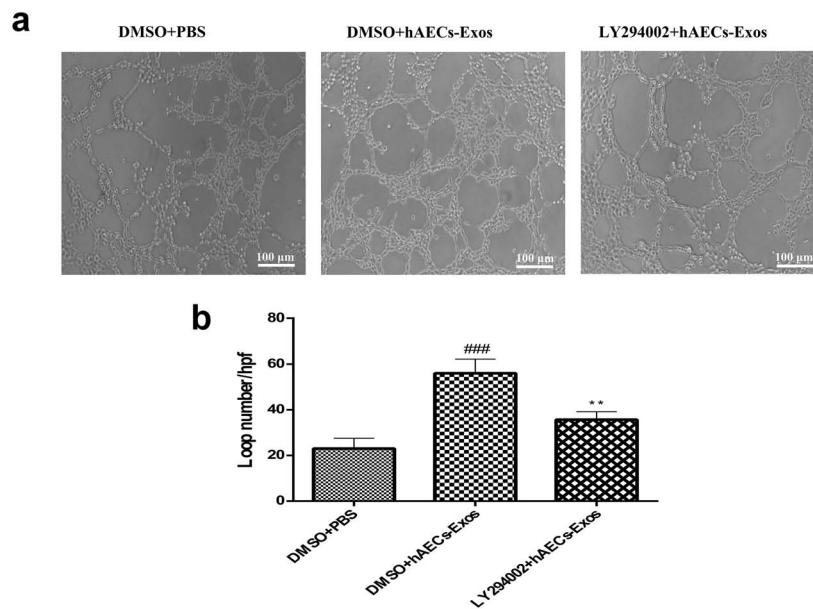

Figure 9. PI3K-AKT-mTOR mediated the tube-formation effects of hAECs-Exos on HUVECs. **(a)** Representative images of the HUVECs tube-formation assay on Matrigel. Scale bars: 100 μm. **(b)** Quantitative analysis of the total loops in HUVECs treated with DMSO + hAECs-Exos, DMSO + PBS and LY294002 + hAECs-Exos. **p < 0.01 compared with DMSO + hAECs-Exos group, ###p < 0.001 compared with the DMSO + PBS group. *PI3K-AKT-mTOR* phosphatidylinositol 3 kinase-protein kinase B-mammalian target of rapamycin, *hAECs-Exos* exosomes derived from human amniotic epithelial cells, *HUVECs* human umbilical vein endothelial cells, *DMSO* Dimethyl Sulfoxide, *PBS* phosphate buffer saline
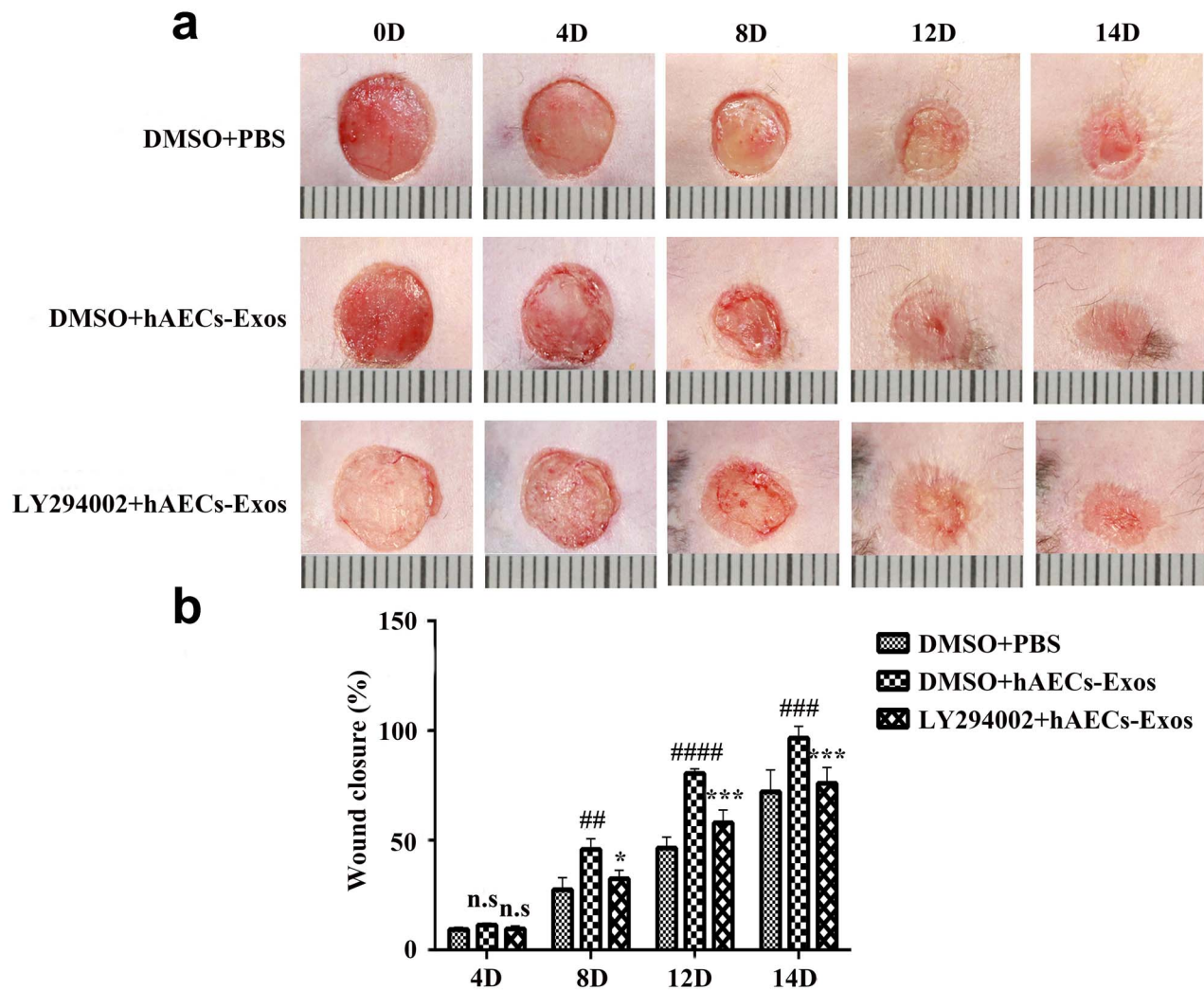
Figure 10. hAECs-Exos accelerated cutaneous wound healing in diabetic mice. **(a)** Gross view of wounds treated with DMSO + hAECs-Exos, DMSO + PBS and LY294002 + hAECs-Exos at days 0, 4, 8, 12 and 14 post-wounding. **(b)** Quantitative analysis of the wound-closure rate for each group at the indicated times. $*p < 0.05$, $***p < 0.001$ compared with DMSO + hAECs-Exos group, $^{\#\#}p < 0.01$ $^{\#\#\#}p < 0.001$, $^{\#\#\#\#}p < 0.0001$ compared with the DMSO + PBS group. $n = 3$ per group. *n.s* no significance, *DMSO* Dimethyl Sulfoxide, *PBS* phosphate buffer saline, *hAECs-Exos* exosomes derived from human amniotic epithelial cells

hAECs-Exos accelerated diabetic wound healing

To explore the effects of hAECs-Exos on diabetic wound healing and the role of the PI3K-AKT-mTOR signaling pathway in this process, two full-thickness cutaneous wounds were created on the backs of db/db mice, followed by subcutaneous injection of DMSO + PBS, hAECs-Exos + DMSO or LY294002 + hAECs-Exos. Digital images of wounds showed much faster wound-closure rates in diabetic mice exposed to hAECs-Exos + DMSO at days 8, 12 and 14 post-wounding when compared with the DMSO + PBS group. However, the pro-wound healing effect was markedly decreased when the PI3K-AKT-mTOR pathway was blocked in local wound tissues (Figure 10). Histological analysis of H&E and Masson's trichrome staining was carried out to evaluate the quality of wound repair. The full thickness of the hAECs-Exos + DMSO group was significantly greater than that of DMSO + PBS group ($p < 0.001$), and markedly

decreased when the PI3K-AKT-mTOR pathway was blocked ($p < 0.05$). Furthermore, in the hAECs-Exos + DMSO group, the dermis collagen was continuous and parallel to the epidermis, and possessed loose and regular arrangement, which was closer to the normal skin structure, as compared with the DMSO + PBS group. The collagen arrangement and deposition in the LY294002 + hAECs-Exos group was somewhere in between (Figure 11). Meanwhile, the mean intensity of immunohistochemical staining for COL 1A1 and COL 3A1 demonstrated that hAECs-Exos remarkably promoted collagen synthesis in the dermis (Figure 12). In addition, the quantification of picrosirius red staining further confirmed the efficiency of hAECs-Exos in promoting collagen deposition (Figure 13). However, when the PI3K-AKT-mTOR pathway was blocked, the beneficial effect of hAECs-Exos on the collagen distribution and deposition were attenuated in the dermis (Figs. 11–13).
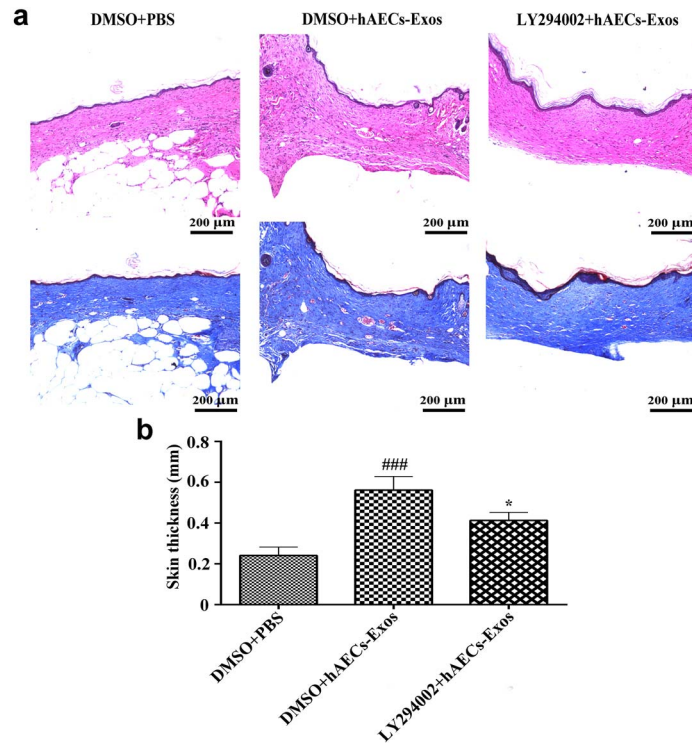
Figure 11. hAECs-Exos facilitated the remodeling of wound healing structure in diabetic mice. **(a)** H&E staining and (middle) Masson's trichrome staining of wound sections treated with DMSO + hAECs-Exos, DMSO + PBS and LY294002 + hAECs-Exos at 18 days after operation. Scale bars: 200 μm. **(b)** Quantitative analysis of the skin thickness in H&E staining. $^*p < 0.05$ compared with DMSO + hAECs-Exos group, $^{###}p < 0.001$ compared with the DMSO + PBS group. $n = 3$ per group. *hAECs-Exos* exosomes derived from human amniotic epithelial cells, *DMSO* Dimethyl Sulfoxide, *PBS* phosphate buffer saline, *H&E* hematoxylin and eosin
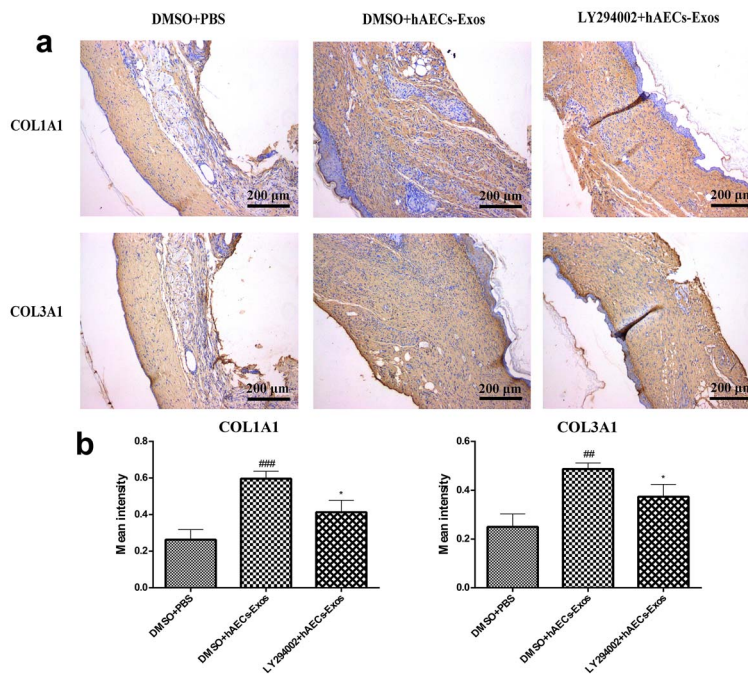

Figure 12. hAECs-Exos facilitated collagen deposition, as demonstrated by immunohistochemistry. **(a)** Immunohistochemical staining for COL 1A1 and 3A1 of wound sections stimulated by DMSO + hAECs-Exos, DMSO + PBS and LY294002 + hAECs-Exos. Scale bars: 200 μm. **(b)** Quantitative analysis of mean intensity of COL 1A1 and 3A1 in **(a)**. $^*p < 0.05$ compared with the DMSO + hAECs-Exos group, $^{##}p < 0.01$, $^{###}p < 0.001$ compared with the DMSO+PBS group. $n = 3$ per group. *DMSO* Dimethyl Sulfoxide, *PBS* phosphate buffer saline, *hAECs-Exos* exosomes derived from human amniotic epithelial cells
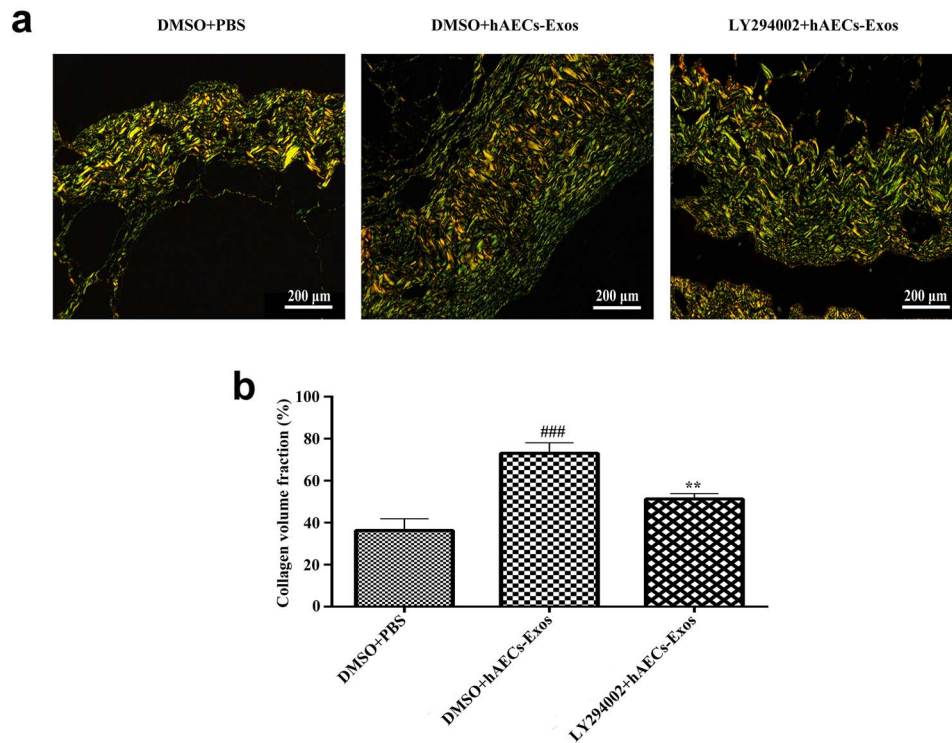
Figure 13. hAECs-Exos inceased the collagen volume fraction, as demonstrated by picrosirius red staining. **(a)** Collagen I and III was detected in wound sections treated with DMSO + hAECs-Exos, DMSO + PBS and LY294002 + hAECs-Exos by picrosirius red staining. Scale bars: 200 μm. **(b)** Statistical analysis of collagen volume fraction for each group. **p < 0.01 compared with DMSO + hAECs-Exos group, ###p < 0.001 compared with the DMSO + PBS group. n = 3 per group. *hAECs-Exos* exosomes derived from human amniotic epithelial cells, *DMSO* Dimethyl Sulfoxide, *PBS* phosphate buffer saline
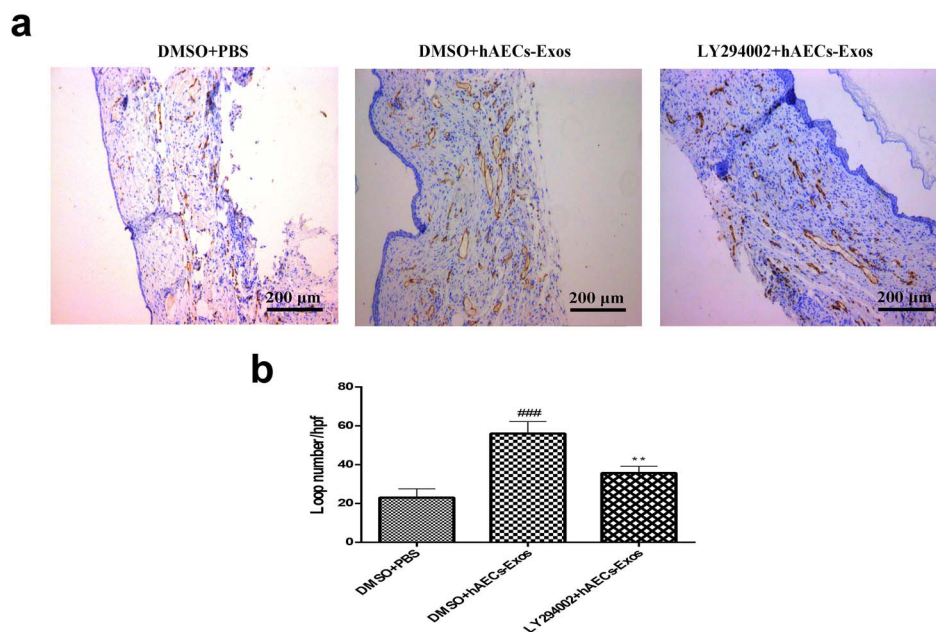

Figure 14. hAECs-Exos increased the capillary density in diabetic wound sites. **(a)** Representative images of the immunohistochemical staining for CD31 in diabetic wound sections treated with DMSO + hAECs-Exos, DMSO + PBS and LY294002 + hAECs-Exos. Scale bars: 200 μm. **(b)** Quantitative analysis of the loop number for each field in every group. **p < 0.01 compared with DMSO + hAECs-Exos group, ###p < 0.001 compared with the DMSO + PBS group. n = 3 per group. *DMSO* Dimethyl Sulfoxide, *PBS* phosphate buffer saline, *hAECs-Exos* exosomes derived from human amniotic epithelial cells

hAECs-Exos increased the capillary density in diabetic wounds sites

CD31 is a widely accepted surface marker of endothelial cells, and so can be used to calculate the tissue capillary density [19]. Immunohistochemical staining for CD31 demonstrated that the capillary density of the hAECs-Exos + DMSO group (56 ± 5.10/hpf) was significantly higher than that in the DMSO+PBS group (23 ± 3.74/hp, $p < 0.001$). When the PI3K-AKT-mTOR pathway was blocked, the number of blood vessels in the LY294002 + hAECs-Exos group (35.67 ± 2.87/hpf) was obviously lower than that in the DMSO + hAECs-Exos group ($p < 0.01$) (Figure 14). These data confirmed that the treatment of hAECs-Exos could increase the formation of new blood vessels in diabetic wounds and that the PI3K-AKT-mTOR signaling pathway is an important pathway for this angiogenesis effect.

Discussion

Although a variety of therapeutic methods have been applied to address diabetic chronic wounds, the optimal therapeutic patterns are still being studied. In this study, we demonstrated that hAECs-Exos could promote the proliferation and migration of HFBs, as well as the angiogenic activity of HUVECs in a high-glucose environment. High-throughput sequencing revealed that hAECs-Exos enriched certain miRNAs that are involved in wound-healing processes. Then, bioinformatics analyses demonstrated that PI3K-AKT was highly enriched and further analyses showed that PI3K-AKT was greatly required for the biological effects of hAECs-Exos on HFBs and HUVECs. *In vivo*, we found that the topical treatment with hAECs-Exos could promote collagen deposition, angiogenesis and the wound-healing process in diabetic mice, whereas these effects were markedly attenuated with the inhibition of PI3K-AKT in wound sites. Our results demonstrate that hAECs-Exos have the ability to deliver wound healing-related miRNAs into HFBs and HUVECs for the activation of the PI3K-AKT pathway, thereby accelerating collagen deposition, revascularization and diabetic wound healing in mice.

Exosome therapy, a cell-free treatment, has become a promising strategy for tissue engineering due to its advantages of low immunogenicity, non-tumorigenicity, high stability, easy acquirement and access to wound sites. To the authors' knowledge, this study is the first to demonstrate that the local transplantation of hAECs-Exos ensured prominent regenerative effects on full-thickness diabetic wounds, which manifested as improved wound-closure rate, collagen deposition, cell proliferation and migration, as well as angiogenesis.

Wound healing is a highly conserved biological process throughout evolution and includes four dynamic processes: the hemostatic stage, inflammation stage, proliferation stage and remolding stage. HFBs, a key cell type in the wound-healing process, secretes a variety of bioactive factors (such as platelet derived growth factor (PDGF), transforming growth factor-β1 (TGF-β1), vascular endothelial growth factor (VEGF), fibroblast growth factor (FGF)) to improve the biological effect of keratinocytes, fibroblasts and vascular endothelial cells and promote the deposition of extracellular matrix, thus facilitating wound healing [18,20]. HFBs derived from diabetic wounds are characterized by abnormal morphology, decreased proliferative activity, inhibited fibroblast-to-myofibroblast differentiation and reduced ability to secrete bioactive factors [21,22]. Numerous studies revealed that enhancing the proliferation, migration and collagen deposition ability of fibroblasts could facilitate cutaneous wound healing [23]. In the present study, we demonstrated that hAECs-Exos could greatly promote the proliferation and migration ability of HFBs and collagen deposition, which ultimately facilitated diabetic wound healing *in vivo*. Although increased collagen deposition may be associated with scar formation, the wound in our current study has just healed completely and has not yet undergone a complete remodeling period. Therefore, it is too early to discuss the relationship between hAECs-Exos and scar formation.

Angiogenesis is another important factor in wound healing, as it provides oxygen and nutrients to the wound sites for tissue generation. Studies have shown that compromised vascularization contributes to delayed diabetic wound healing and promoting the function of endothelial cells could accelerate this [24]. Moreover, our previous study demonstrated that hAECs could promote neovascularization in diabetic wounds through paracrine factors [5]. However, whether hAECs-Exos could increase angiogenesis has not been reported before. In this study, we found that hAECs-Exos strongly promoted the angiogenic activity of HUVECs in a high-glucose environment and increased the capillary density in hAECs-Exo-treated diabetic wounds. The results suggest that the pro-wound healing action of hAECs-Exos is likely partially attributable to its pro-angiogenic effect.

The group of miRNAs is a short non-coding RNA with a length of about 20–24 nucleotides and regulates nearly one-third of human genes via binding to the 3' untranslated regions (3' UTRs) of their target mRNAs [25]. A large number of studies have shown that miRNAs are the primary effective cargo of exosomes [11,18,26,27]. In addition, Zhao *et al*. [28] confirmed that hAECs could promote the healing of acute wounds through specific miRNAs rather than proteins or other particles. So, in order to explore the underlying mechanism of the beneficial effects of hAECs-Exos on HFBs and HUVECs, we carried out high-throughput sequencing of the miRNA landscape in hAECs-Exos. Results demonstrated that many miRNAs in the miRNA spectrum of hAECs-Exos are highly related to the wound-healing process. For example, previous studies have shown that miRNA-21 is upregulated during acute wound healing, but significantly decreased during diabetic wound healing [29]. Overexpression of miRNA-21 in HFBs, endothelial cells and keratinocytes could significantly facilitate wound healing

[30,31]. In addition, both miR-99 and miR-26a-5p have also been reported to promote tissue regeneration [32,33]. In the present study, we found that hAECs-Exos-miRNAs could be successfully transferred into HFBs and HUVECs in their mature form, as tested by RT-qPCR. Therefore, hAECs-Exos-miRNAs may partly explain the beneficial effects of hAECs-Exos on HFBs and HUVECs. Unfortunately, when transfecting corresponding mimics of the enrichment and interesting miRNAs into HFBs and HUVECs, we did not find any single miRNA that could play a significant role in the angiogenesis and function of HFBs. Therefore, we assume that each single miRNA probably cannot recapitulate the functions of hAEC-Exos on HFBs and HUVECs and that they may form a cluster or function in concert to mediate the observed phenotype, which we will further confirm in follow-up studies.

In order to explore the mechanism of action of hAEC-Exos, both KEGG and GO analyses were further performed to identify enriched signaling pathways and biological processes of target genes for the top 15 miRNAs in hAECs-Exos. Results demonstrated that the PI3K-AKT signaling pathway was highly enriched, and the activation of this pathways in HFBs and HUVECs treated with hAECs-Exos was further confirmed by western blotting. As known, according to the structural characteristics and substrate specificity, PI3K is divided into three classes (class I, II and III). Among them, the class I molecular pathway, PI3K-AKT-mTOR, is critical for cell proliferation, motility, metabolism and tumorigenesis, and plays great roles in promoting wound healing [10,34,35]. In our study, we discovered that p-AKT and p-mTOR were extremely highly expressed in HFBs and HUVECs treated with hAECs-Exos and that this expression tendency is inhibited by LY204002, as demonstrated by the western blotting results. Meanwhile, when the PI3K-AKT-mTOR signaling pathway was inhibited in HFBs and HUVECs, the beneficial effects of hAECs-Exos on the function of HFBs and HUVECs, both *in vitro* and *in vivo*, were all greatly suppressed. Given these findings, the results of our study confirmed that hAECs-Exos could enhance the biological function of HFBs and HUVECs and facilitate would healing process through the PI3K-AKT-mTOR signaling pathway. Once this pathway was inhibited, all the effects were compromised. Therefore, PI3K-AKT-mTOR is a critical mediator for the beneficial effects of hAECs-Exos on diabetic wound healing. However, it should be stressed that the effects of hAECs-Exos on the function of HFBs and HUVECs, as well as on wound healing *in vivo*, were not entirely abolished by PI3K-AKT-mTOR inhibition, suggesting that other signaling pathways may also be involved in these processes. Thus, PI3K-AKT-mTOR is one of the important pathways that mediates the wound-healing effects of hAECs-Exos, but not the only one.

Although we determined that PI3K-AKT-mTOR activated by hAECs-Exos-miRNAs contributed to the beneficial effects of hAECs-Exos on diabetic wound healing, the present study has limitations. First, the degree of PI3K-AKT-mTOR function in diabetic wound healing is not yet known, so how much of a role it plays still needs to be elucidated. Second, while some potential miRNAs have been found to explain the biological effects of hAECs-Exos, further studies are still necessary to identify the key miRNAs. Moreover, whether continuous and large-dose delivery of hAECs-Exos could induce better pro-regenerative effects on diabetic wound healing requires further exploration.

Conclusion

In summary, our findings confirmed that hAECs-Exos could effectively promote the biological properties of HFBs and HUVECs in a high-glycemic environment, as well as facilitate diabetic wound healing in mice. The PI3K-AKT-mTOR pathway plays a crucial role in this process and all these beneficial effects can be weakened by PI3K-AKT-mTOR inhibition. Our findings suggest that hAECs-Exos may represent a promising strategy for diabetic wound healing by promoting angiogenesis and fibroblast function via activation of the PI3K-AKT-mTOR pathway.

Availability of data and materials

The datasets used and analysed are available from the corresponding author on reasonable request.

Authors' contributions

Zhaohong Chen, Yongjun Zheng and Zhaofan Xia conceived and designed the study; Pei Wei, Li Li and Pengfei Luo consulted the literature and prepared materials; Chenjian Zhong, Xiaolan Yang, Futing Shu and Teng Gong offered technical support; Pei Wei and Yongjun Zheng performed the experiment and analysed the data; Pei Wei wrote the paper; Yongjun Zheng, Zhaohong Chen, Pengfei Luo and Zhaofan Xia revised the paper.

Ethics approval and consent to participate

All participants in this study signed written informed consent and all procedures were approved by the Ethics Committee of

Changhai Hospital, Shanghai, China. Animals involved in this study was approved by the Ethics Committee of Naval Medical University Experimental Animal Center and were handled according to international animal welfare standards.

Conflicts of interest

The authors declare that they have no competing interests.

Abbreviations

hAECs: human amniotic epithelial cells; miRNA: micro RNA; HFBs: human fibroblasts; HUVECs: human umbilical vein endothelial cells; hAEC-Exos: exosomes derived from human amniotic epithelial cells; DMEM: Dulbecco's modified Eagle's medium; FBS: fetal bovine serum; PBS: phosphate buffered saline; DLS: dynamic light scattering; TEM: transmission electron microscope; FCM: flow cytometry; PI3K: phosphatidylinositol 3 kinase; AKT: protein kinase B; DMSO: dimethyl sulfoxide; CCK-8: cell counting kit-8; mTOR; mammalian target of rapamycin; KEGG: Kyoto Encyclopedia of Genes and Genomes; GO: Gene Ontology; H&E: hematoxylin-eosin; SD: standard deviation; ANOVA: analysis of variance

References

1. Patel S, Srivastava S, Singh MR, Singh D. Mechanistic insight into diabetic wounds: pathogenesis, molecular targets and treatment strategies to pace wound healing. *Biomed Pharmacother*. 2019. doi: 10.1016/j.biopha.2019.108615.

2. Snyder RJ, Kirsner RS, Warriner RA, Lavery LA, Hanft JR, Sheehan P. Consensus recommendations on advancing the standard of care for treating neuropathic foot ulcers in patients with diabetes. *Ostomy Wound Manage*. 2010;56:S1–24.

3. Azar ND, Fatemeh MB, Mohammad C, Shiva RD. Skin tissue engineering: wound healing based on stem-cell-based therapeutic strategies. *Stem Cell Res Ther*. 2019. doi: 10.1186/s13287-019-1212-2.

4. Akle CA, Adinolfi M, Welsh KI, Leibowitz S, Mccoll I. Immunogenicity of human amniotic epithelial cells after transplantation into volunteers. *Lancet*. 1981;2:1003–5.

5. Zheng Y, Zheng S, Fan X, Li L, Xiao Y, Luo P, et al. Amniotic epithelial cells accelerate diabetic wound healing by modulating inflammation and promoting neovascularization. *Stem Cells Int*. 2018. doi: 10.1155/2018/1082076.

6. Herberts CA, Kwa MS, Hermsen HP. Risk factors in the development of stem cell therapy. *J Transl Med*. 2011;9:29.

7. Cabral J, Ryan A, Griffin M, Ritter T. Extracellular vesicles as modulators of wound healing. *Adv Drug Deli Rev*. 2018;129:394–406.

8. Gurunathan S, Kang M, Jeyaraj M, Qasim M, Kim J. Review of the isolation, characterization, biological function, and multifarious therapeutic approaches of Exosomes. *Cells*. 2019;8:307–43.

9. Yang X, Sun C, Wang L, Guo X. New insight into isolation, identification techniques and medical applications of exosomes. *Cell*. 2019;308:119–29.

10. Zhang J, Chen C, Hu B, Niu X, Liu X, Zhang G, et al. Exosomes derived from human endothelial progenitor cells accelerate cutaneous wound healing by promoting angiogenesis through Erk1/2 signaling. *Int J Biol Sci*. 2016;12:1472–87.

11. Hu Y, Rao S, Wang Z, Cao J, Tan Y, Luo J, et al. Exosomes from human umbilical cord blood accelerate cutaneous wound healing through miR-21-3p-mediated promotion of angiogenesis and fibroblast function. *Theranostics*. 2018;8: 169–84.

12. Shabbir A, Cox A, Rodriguez-Menocal L, Salgado M, Badiavas EV. Mesenchymal stem cell Exosomes induce proliferation and migration of normal and chronic wound fibroblasts, and enhance angiogenesis in vitro. *Stem Cells Dev*. 2015; 24:1635–47.

13. Hu P, Yang Q, Wang Q, Shi C, Wang D, Armato U, et al. Mesenchymal stromal cells-exosomes: a promising cell-free therapeutic tool for wound healing and cutaneous regeneration. *Burns Trauma*. 2019. doi: 10.1186/s41038-019-0178-8.

14. Zheng Y, Ji S, Wu H, Tian S, Wang X, Luo P, et al. Acceleration of diabetic wound healing by a cryopreserved living dermal substitute created by micronized amnion seeded with fibroblasts. *Am J Transl Res*. 2015;7:2683–93.

15. Lv C, Duan H, Wang S, Gan L, Xu Q. Exosomes derived from human umbilical cord Mesenchymal stem cells promote proliferation of allogeneic endometrial stromal cells. *Reprod Sci*. 2020;27:1372–81.

16. Zheng Y, Wang X, Ji S, Tian S, Wu H, Luo P, et al. Mepenzolate bromide promotes diabetic wound healing by modulating inflammation and oxidative stress. *Am J Transl Res*. 2016;8:2738–47.

17. Liu T, Qiu C, Ben C, Li H, Zhu S. One-step approach for full-thickness skin defect reconstruction in rats using minced split-thickness skin grafts with Pelnac overlay. *Burns Trauma*. 2019. doi: 10.1186/s41038-019-0157-0.

18. Fang S, Xu C, Zhang Y, Xue C, Yang C, Bi H, et al. Umbilical cord-derived Mesenchymal stem cell-derived Exosomal MicroRNAs suppress Myofibroblast differentiation by inhibiting the transforming growth factor-*β*/SMAD2 pathway during wound healing. *Stem Cell Transl Med*. 2016;5:1425–39.

19. Liu M, Liu T, Zhang X, Jian Z, Xia H, Yang J, et al. Fabrication of KR-12 peptide-containing hyaluronic acid immobilized fibrous eggshell membrane effectively kills multi-drug-resistant bacteria, promotes angiogenesis and accelerates re-epithelialization. *Int J Nanomed*. 2019;14:3345–60.

20. Darby IA, Laverdet B, Bonté F, Desmouliére A. Fibroblasts and myofibroblasts in wound healing. *Clin Cosmet Investig Dermatol*. 2014;7:301–11.

21. Khamaisi M, Katagiri S, Keenan H, Park K, Maeda Y, Li Q, et al. PKCδ inhibition normalizes the wound-healing capacity of diabetic human fibroblasts. *J. Clin. Investig*. 2016;126: 837–53.

22. Loots MA, Lamme EN, Mekkes JR, Bos JD, Middelkoop E. Cultured fibroblasts from chronic diabetic wounds on the lower extremity (non-insulin-dependent diabetes mellitus) show disturbed proliferation. *Arch Dermatol Res*. 1999;291:93–9.

23. Mizoguchi T, Ueno K, Yanagihara M, Samura M, Kurazumi H, Suzuki R, et al. Autologous fibroblasts, peripheral blood mononuclear cells, and fibrin glue accelerate healing of refractory cutaneous ulcers in diabetic mice. *Am J Transl Res*. 2018;10:2920–8.

24. Martin A, Komada MR, Sane DC. Abnormal angiogenesis in diabetes mellitus. *Med Res Rev*. 2003;23:117–45.

25. Syed SN, Brüne B. MicroRNAs as emerging regulators of signaling in the tumor microenvironment. *Cancers*. 2020;12: 911.

26. Xiao G, Cheng C, Chiang Y, Cheng W, Liu I, Wu S. Exosomal miR-10a derived from amniotic fluid stem cells preserves ovarian follicles after chemotherapy. *Sci Rep*. 2016;6:23120.

27. Fortunato O, Gasparini P, Boeri M, *et al*. Exo-microRNAs as a new tool for liquid biopsy in lung cancer. *Cancers*. 2019;11:888–903.

28. Zhao B, Li X, Shi X, Shi X, Zhang W, Wu G, *et al*. Exosomal MicroRNAs derived from human amniotic epithelial cells accelerate wound healing by promoting the proliferation and migration of fibroblasts. *Stem Cells Int*. 2018. doi: 10.1155/2018/5420463.

29. Yang X, Wang J, Guo S, Fan K, Li J, Wang Y, *et al*. miR-21 promotes keratinocyte migration and re-epithelialization during wound healing. *Int J Biol Sci*. 2011;7:685–90.

30. Wang T, Feng Y, Sun H, Zhang L, Hao L, Shi C, *et al*. miR-21 regulates skin wound healing by targeting multiple aspects of the healing process. *Am J Pathol*. 2012;181:1911–20.

31. Madhyastha R, Madhyastha H, Nakajima Y, Omura S, Maruyama M. MicroRNA signature in diabetic wound healing: promotive role of miR-21 in fibroblast migration. *Int Wound J*. 2012;9:355–61.

32. Jin Y, Tymen SD, Chen D, Fang ZJ, Zhao Y, Dragas D, *et al*. MicroRNA-99 family targets AKT/mTOR signaling pathway in dermal wound healing. *PLoS One*. 2013:e64434–42. doi: 10.1371/journal.pone.0064434.

33. Xiong Y, Cao F, Hu L, Yan C, Chen L, Panayi AC, *et al*. microRNAs-26a-5p accelerates healing via Downregulation of PTEN in fracture patients with traumatic brain injury. *Mol Ther-Nucl Acids*. 2019;17:223–34.

34. Zhang E, Gao B, Yang L, Wu X, Wang Z. Notoginsenoside Ft1 promotes fibroblast proliferation via PI3K/Akt/mTOR signaling pathway and benefits wound healing in genetically diabetic mice. *J Pharmacol Exp Ther*. 2016;356: 324–32.

35. Xiao W, Tang H, Wu M, Liao Y, Li K, Li L, *et al*. Ozone oil promotes wound healing by increasing the migration of fibroblasts via PI3K/Akt/mTOR signaling pathway. *Bioscience Rep*. 2017. doi: 10.1042/BSR20170658.